Inorganic Chemistry

Article

pubs.acs.org/IC

A New Class of Cuprous Bromide Cluster-Based Hybrid Materials: Direct Observation of the Stepwise Replacement of Hydrogen Bonds by Coordination Bonds

Xian-Ming Zhang,* Juan-Juan Hou, Cai-Hong Guo, and Chun-Fang Li

School of Chemistry & Material Science, Shanxi Normal University, Linfen 041004, P. R. China

Supporting Information

ABSTRACT: Although a variety of functional metal−organic frameworks (MOFs) have been synthesized, post-modified, and applied in various areas, there is little knowledge about how molecular cluster building units are stepwise evolved into MOFs via intermediates. Coordination bonds are generally stronger than hydrogen bonds, and thus equivalent replacement of X−H···Y hydrogen bonds by X−M−Y coordination bonds can transform hydrogen bond networks into MOFs. In this work, solvothermal in situ reduction reactions of $CuBr_2$ and 1,4-diazoniabicyclo[2,2,2]octane (DABCO) generated a myriad of tunable photoluminescent cuprous body-centered cubic bromide cluster-based networks with the general formula $[Cu_{4+x}H_{4-x}Br_6(DABCO)_4](HCO_2)_2{\cdot}S$ (x = 0, 0.56, 0.81, 1.27, 1.39, 2.56, 2.78, and 4 for compounds **1**−**8**, respectively). All of these compounds crystallize in the cubic space group with the largest volume difference being only 5.2%, but they belong to three remarkably different kinds of crystals. Complex **1** is a molecular crystal and consists of tetrahedral $[Cu_4Br_6(HDABCO)_4]^{2+}$ clusters with monodentate HDABCO groups that are supported via N−H···Br synthons in the hydrogen bond network. Compound **8** is a $[Cu_8Br_6]^{2+}$ cube cluster-based MOF with bridged DABCO ligands. Complexes **2**−**7** are seemingly impossible Cu/H-substituted solid solutions of **1** and **8**. The CuBr framework components in **1**−**8** are Cu_4Br_6, $Cu_{4.56}Br_6$, $Cu_{4.81}Br_6$, $Cu_{5.27}Br_6$, $Cu_{5.39}Br_6$, $Cu_{6.56}Br_6$, $Cu_{6.78}Br_6$, and Cu_8Br_6, respectively. Crystallization kinetics studies revealed that the $[Cu_4Br_6(HDABCO)_4]^{2+}$ cluster-based hydrogen bond network (**1**) was initially formed such that N−H···Br hydrogen bonds could be stepwise replaced by N−Cu−Br coordination bonds to form the $[Cu_8Br_6]^{2+}$ cube cluster-based MOF (**8**) via solid solutions. These observations directly reveal the equivalence and transformation between the N−H···Br hydrogen bond and the N−Cu−Br coordination bond and the evolutionary mechanism of a molecular crystal to a MOF via solid solutions, which is of fundamental importance in materials but has never before been revealed. DFT calculations suggest that equivalent replacement of a N−H···Br hydrogen bond by a N−Cu−Br coordination bond is exothermic and exergonic, which also supports the transformation from molecule **1** to MOF **8**.

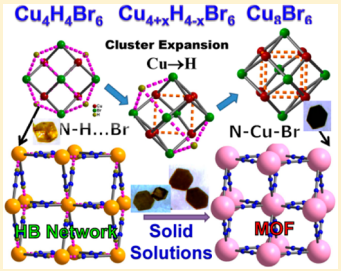

INTRODUCTION

The primary concern in the rational design of crystalline metal−organic framework (MOF) materials is predictability and/or tunable properties from well-designed molecular cluster units[1], which have undergone remarkable growth, with applications in areas such as energy storage, environmental chemistry, catalysis, electronics, chirality, pharmaceutics, and solid-state synthesis.[2] Particularly relevant is the recently developed postsynthesized strategy that allows functionalities of MOFs to be chemically altered for use.[3] To date, a variety of MOFs have been synthesized and post-modified,[2,4] but there is little knowledge about the mechanism underlying how molecular cluster building units are step-by-step evolved into MOFs via intermediates.[5,6] In general, molecular cluster units in molecular crystals are separable, being linked via hydrogen bonds into hydrogen bond networks. In contrast, molecular cluster units in MOFs are inseparable, being linked via coordination bonds into metal coordination frameworks.[7] Postsynthesized modification of crystals involves cooperative movement of atoms in the solid state, which could be a useful strategy for tuning material properties.[8] Recently, insertion and exchange of coordinate cations, even via crystal to crystal transformation, have been achieved through postsynthesized treatment of crystals.[9] Coordination bonds are generally stronger than hydrogen bonds, and thus the equivalent replacement of X−H···Y hydrogen bonds by X−M−Y coordination bonds will transform a hydrogen bond network into a MOF, which is of fundamental importance but has never been revealed in a single crystal to single crystal manner.

On the other hand, a burgeoning area in the field of crystal engineering involves the design of multicomponent solids, such as solid solutions and cocrystals, because they possess new or superior properties relative to those of the individual components.[10,11] Solid solutions, commonly formed in inorganic solids via substitution of adjacent metal elements,[12] are relatively less explored in molecular crystals and MOFs because of their different lattice and crystallization kinetics.[13] On the basis of organic ligand incorporation, solid solutions in molecular crystals and MOFs can be generated via substitution of metals as well as organic ligands. To date, substitutional metal elements are close together on the periodic table, and

Received: October 1, 2014
Published: December 29, 2014

DOI: 10.1021/ic5024168
Inorg. Chem. 2015, 54, 554−559

substitutional ligands have similar structures and functional groups among solid solutions of molecular crystals and MOFs.[14] The metal copper and the nonmetal hydrogen are quite separate on the periodic table, and their covalent radii are quite different. It seems impossible that substitution of H for Cu could form solid solutions of coordination compounds.[15] However, the unique X−H···Y hydrogen bonding nature of the hydrogen element can sometimes give equivalent functionality of H in X−H···Y and Cu(I) in X−Cu−Y bonds,[16] which forms the foundation of Cu- and H-substituted multicomponent solids (Chart 1).

Chart 1. View of the Counterpart between the N−H···Br Synthon and the N−Cu−Br Bond in this Article[a]

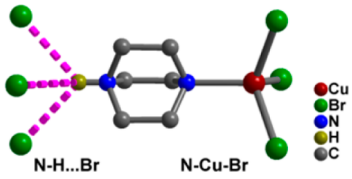

[a] Both H and Cu are tetrahedrally bonded to one N and three Br atoms.

In this Article, we present a myriad of body-centered cubic tunable photoluminescent cuprous bromide networks, namely $[Cu_{4+x}H_{4-x}Br_6(DABCO)_4](HCO_2)_2{\cdot}S$ (DABCO = 1,4-diazoniabicyclo[2,2,2]octane) (x = 0, 0.56, 0.81, 1.27, 1.39, 2.56, 2.78, and 4 for **1**−**8**, respectively), and reveal the stepwise evolution of metal clusters to MOFs via seemingly impossible solid solutions. All eight compounds crystallize in body-centered cubic space groups, and the cell volumes are only increased by 5.2%. Complex **1** consists of isolated tetrahedral $[Cu_4Br_6(HDABCO)_4]^{2+}$ clusters that are extended via N−H···Br hydrogen bond synthons into a body-centered cubic hydrogen bond network. Complex **8** is a body-centered cubic MOF constructed of $[Cu_8Br_6]^{2+}$ cube clusters and bridged DABCO ligands. Complexes **2**−**7** are seemingly impossible solid solutions of **1** and **8**. Experimental and theoretical studies on crystallization and transformation mechanisms revealed that hydrogen bond network **1** with high energy $Cu_4Br_6^{2-}$ clusters was formed initially in which N−H···Br hydrogen bonds could be replaced by N−Cu−Br coordination bonds to form MOF **8** via solid solution intermediates. These compounds show tunable yellow-to-red photoluminescence due to the superior properties of multicomponent solids.

EXPERIMENTAL SECTION

Materials and Methods. Fourier transform infrared (FT-IR) spectra were recorded from KBr pellets in the range of 400−4000 cm^{-1} on a PerkinElmer Spectrum BX FT-IR spectrometer. Elemental analysis was performed on a Vario EL III elemental analyzer. X-ray powder diffraction (XRPD) data were recorded on a Bruker D8 ADVANCE X-ray powder diffractometer (Cu Kα, λ = 1.5418 Å). Scanning electron microscope energy-dispersive X-ray spectroscopy (SEM-EDS) analyses were conducted on a JSM-7500F SEM equipped with an EDAX CDU leap detector. Thermal analyses were carried out in air atmosphere using SETARAM LABSYS equipment with a heating rate of 10 °C/min. Photoluminescence analyses were performed on an Edinburgh FLS920 luminescence spectrometer.

Syntheses. A mixture of $CuBr_2$ (0.135 g, 0.6 mmol), DABCO·$6H_2O$ (0.085 g, 0.3 mmol), DMF (4 mL), and H_2O (3 mL) was stirred in air. The resulting solution was transferred into a 15 mL Teflon-lined stainless steel reactor, which was heated at 85 °C for 72 h. After the solution was cooled to room temperature, pale yellow crystals of **1** and **2** were recovered in 45 and 15% yield, respectively. When the reaction time was increased from 72 h, approximate mixed crystals of **1**−**4** (96 h), **2**−**7** (120 h), **3**−**8** (144 h), **5**−**8** (168 h), and **7** and **8** (240 h) were recovered with different relative yields. When the reaction time was increased to 360 h, single phase crystals of **8** were obtained. The colors of crystals **1**−**8** deepen from pale yellow to brown. Because of their coexistence within a certain distribution range, mixed crystals of **2**−**7** could not be completely separated. However, changing certain reaction parameters, such as the solvent and reaction temperature, can produce single phase crystals of **1** and **8**. For example, solvothermal treatment of a mixture of $CuBr_2$ (0.135 g, 0.6 mmol), DABCO·$6H_2O$ (0.085 g, 0.3 mmol), DMF (1 mL), and H_2O (6 mL) at 140 °C for 120 h gave single phase crystals of **1** in 45% yield. Solvothermal treatment of a mixture of $CuBr_2$ (0.135 g, 0.6 mmol), DABCO·$6H_2O$ (0.085 g, 0.3 mmol), and DMF (7 mL) at 160 °C for 120 h generated single phase crystals of **8** in 64% yield. Anal. Calcd for **1**: C, 23.93; H, 4.71; N, 8.59. Found: C, 23.74; H, 4.95; N, 8.34. Anal. Calcd for **8**: C, 19.69; H, 3.50; N, 7.07. Found: C, 19.88; H, 3.78; N, 7.74.

X-ray Crystallography. Single crystals of **1**−**8** were used in intensity data collection using a Bruker SMARTAPEX CCD diffractometer at 298(2) K (λ = 0.71073 Å). The structure was solved by direct methods and refined by full-matrix least-squares methods with SHELXTL. The occupancy of Cu sites was set to the free mode. All non-hydrogen atoms were refined with anisotropic thermal parameters.

Calculation Details. Density functional theory (DFT) and time-dependent DFT (TD-DFT) calculations were performed using the B3LYP functional. The LANL2DZ basis sets were employed for Cu and Br. The initial ground-state models obtained from the X-ray and modified structural models were optimized. All calculations were performed with the Gaussian09 software package.[17] Dimensional plots of molecular configurations and orbitals were generated with the GaussView program.

DISCUSSION

Description of Structures. Compound **1** crystallizes in space group *I*-43*m* and consists of a crystallographically independent asymmetric unit containing one Cu, one Br, and 1/6 singly protonated HDABCO. The Cu atom has 3*m* symmetry (*Wyckoff letter* 8c) tetrahedrally coordinated by three Br atoms and one N atom from one singly protonated HDABCO molecule.

The Cu−Br bond lengths are 2.4768(15) Å, whereas the Cu−N bond length is 2.15(3) Å. The L−Cu−L angles are in the range of 108.08(10)−110.83(9)°. Four Cu and six μ_2-Br atoms form a T_d symmetric Cu_4Br_6 cluster with a perfect (μ-$Br)_6$ octahedron and Cu_4 tetrahedron (Figure 1). The Cu···Cu distance within Cu_4Br_6 is ∼3.97 Å, and Cu−Cu−Cu and Br−

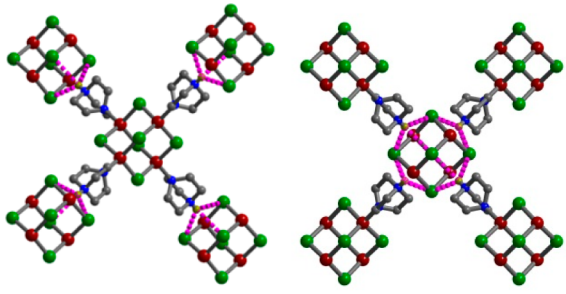

Figure 1. View of each $[Cu_4(\mu\text{-}Br)_6(HDABCO)_4]^{2+}$ as hydrogen donors (left) and acceptors (right) being linked to four neighbors via N−H···Br hydrogen bond synthons. H···Br interactions in N−H···Br hydrogen bonds are shown in a dashed purple color.

DOI: 10.1021/ic5024168
Inorg. Chem. 2015, 54, 554−559

Br−Br angles are exactly 60°. The Cu_4Br_6 geometry is quite different from that in $[P(C_4H_9)(C_6H_5)_3]_2[Cu_4Br_6]$, where discrete $[Cu_4Br_6]^{2-}$ clusters have trigonal-planar coordinated Cu(I) atoms (Cu−Cu, 2.74 Å).[18] The Cu_4Br_6 in **1** is further coordinated by four singly protonated HDABCO groups to form a $[Cu_4Br_6(HDABCO)_4]^{2+}$ cluster. Each H atom of HDABCO is bonded to three bromides to form a charge-assisted hydrogen synthon; the N···Br distance in a N−H···Br hydrogen bond is 3.67 Å, and the N−H···Br angle is 129.1°. Each $[Cu_4Br_6(HDABCO)_4]^{2+}$ cluster acts as a N−H···Br hydrogen bond acceptor for four clusters and donor for an additional four clusters.[19] The overall structure is a three-dimensional (3D) body-centered cubic hydrogen bond network with channels filled by formates and water molecules (Figure 2). The topology is bcu with a Schläfli symbol of $4^{24}6^4$.[20] The

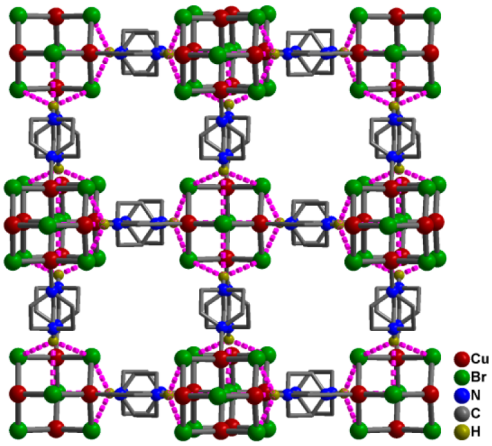

Figure 2. View of the body-centered cubic hydrogen bond network constructed by $[Cu_4(\mu\text{-}Br)_6(HDABCO)_4]^{2+}$ clusters via N−H···Br hydrogen bonds in **1**. The H···Br interactions are shown in a dashed purple color.

charge-assisted hydrogen bond interactions in **1** involve the Columbic field[16,21] and are robust, transferable, and suitable for molecular crystal engineering.

For a better understanding of the structures of **2**−**7**, the structure of **8** should be preferentially described. Compared to **1**, compound **8** is higher, crystallizing in cubic space group *Im*-3*m*. The *a*-axis length is 13.6261(4) Å, and the cell volume is 2529.97(13) Å^3, which are increased by 1.8 and 5.2% compared with those of **1**, respectively. The crystallographically independent asymmetric unit consists of one Cu, one Br, and 1/12 DABCO. The Cu atom has 3*m* symmetry (*Wyckoff letter* 16f) coordinated by three Br atoms and one N atom from DABCO. The Cu−Br bond lengths are 2.5218(16) Å, whereas the Cu−N bond lengths are 2.097(14) Å. The L−Cu−L angles are in the range of 109.37(6)−109.58(6)°. Remarkably, eight Cu and six μ_4-Br atoms form a perfect O_h symmetric Cu_8Br_6 cube cluster,[22] which can be viewed as the result of interpenetration of a $(\mu_4\text{-}Br)_6$ octahedron by a Cu_8 cube. The short Cu···Cu distance within a Cu_8Br_6 cube is 2.916(3) Å, and Cu−Cu−Cu angles are exactly 90°. The $[Cu_8Br_6]^{2+}$ cluster is coordinated by nitrogen atoms of bridged DABCO groups, and the N···Br distance in the N−Cu−Br bond is 3.78 Å, which is only 0.11 Å larger than the N···Br distance of 3.67 Å in the N−H···Br hydrogen synthon in **1**. Each $[Cu_8Br_6]^{2+}$ cluster is linked to eight neighbors via bridged DABCO groups to form 3D body-centered cubic MOFs with channels filled by formates and water molecules (Figure 3).

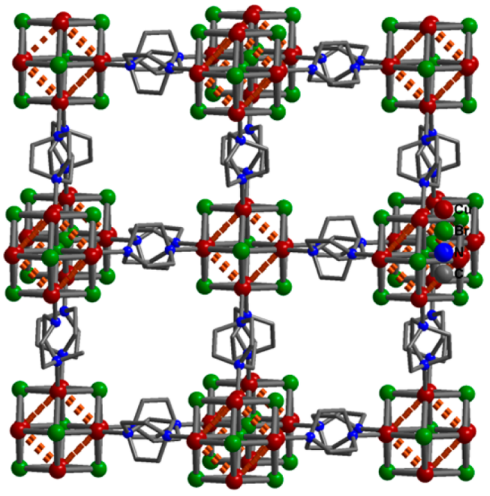

Figure 3. View of body-centered cubic MOF constructed by $[Cu_8(\mu_4\text{-}Br)_6]^{2+}$ cube clusters via bridged DABCO groups in **8**. The short Cu···Cu interactions are shown in a dashed brown color.

Most surprisingly, compounds **2**−**7** are solid solutions of hydrogen bond network **1** and MOF **8**. Compounds **2** and **3** also crystallize in space group *I*-43*m*, and the asymmetric unit consists of two crystallographically independent copper atoms with 3*m* symmetry. In **2** and **3**, both independent Cu sites are partially occupied, and the final refinement shows that the Cu(1) site is approximately 89.9 and 71.2% occupied, respectively, whereas the Cu(2) site is 23.9 and 49.1% occupied, respectively. This gives rise to a Cu:Br molar ratio of $Cu_{4.56}Br_6$ and $Cu_{4.81}Br_6$ in **2** and **3**, respectively, which is largely in agreement with the EDS data. Compounds **4**−**7** crystallize in space group *Im*-3*m*, and the asymmetric unit consists of one crystallographically independent Cu similar to **8**. However, the independent Cu site is partially occupied by 64.7, 67.4, 83.2, and 84.8% in **4**−**7**, respectively, as determined by the final refinement, which is different from the case in **8**. This gives rise to CuBr components of $Cu_{5.27}Br_6$, $Cu_{5.39}Br_6$, $Cu_{6.56}Br_6$, and $Cu_{6.78}Br_6$ in **4**−**7**, respectively (Table 1). Considering partially

Table 1. Crystal Data Showing a Gradual Increase in Cu:Br Ratio with Increased Cell Volume in 1−8

compound	space group	*a* (Å)	*V* (Å^3)	Cu:Br ratio
1	*I*-43*m*	13.3863(6)	2398.73(19)	Cu_4Br_6
2	*I*-43*m*	13.4124(7)	2412.8(2)	$Cu_{4.56}Br_6$
3	*I*-43*m*	13.4488(3)	2432.49(9)	$Cu_{4.81}Br_6$
4	*Im*-3*m*	13.4786(3)	2448.69(9)	$Cu_{5.27}Br_6$
5	*Im*-3*m*	13.5186(3)	2470.56(9)	$Cu_{5.39}Br_6$
6	*Im*-3*m*	13.5838(4)	2506.48(13)	$Cu_{6.56}Br_6$
7	*Im*-3*m*	13.5926(5)	2511.35(16)	$Cu_{6.78}Br_6$
8	*Im*-3*m*	13.6261(4)	2529.97(13)	Cu_8Br_6

occupied Cu sites, **2**−**7** appear to also contain Cu_8Br_6 cubes similar to those in **8**. The N···Br distances of N−Cu−Br bonds in **2**−**7** are ∼3.70 Å, a value between 3.67 Å in the hydrogen bond network of **1** and 3.78 Å in the MOF of **8**. Considering the partial occupancy of Cu sites and the intrinsic average structures determined by X-ray diffraction, Cu_5Br_6, Cu_6Br_6, and Cu_7Br_6 clusters should exist in **2**−**7**. The equivalence between

DOI: 10.1021/ic5024168
Inorg. Chem. 2015, 54, 554−559

N−H···Br and N−Cu−Br bonds also indicates that Cu-deficient sites in local Cu_8Br_8 clusters are compensated by H atoms from protonated HDABCO groups. The DABCO groups in **2**−**7** exist as singly protonated HDABCO and nonprotonated DABCO molecules. In total, the structures of **2**−**7** are best described as Cu/H-substituted solid solutions of a hydrogen bond network of $[Cu_4Br_6(HDABCO)_4]^{2+}$ and a MOF of $[Cu_8Br_6(DABCO)_4]^{2+}$. Nominally, the formation of solid solutions of **2**−**7** can be viewed as the replacement of H atoms of N−H···Br bonds in **1** by Cu atoms accompanied by generation of N−Cu−Br bonds (Figure 4). Metal Cu and nonmetal H have a large difference in their covalent radii, and discovery of the highly unusual Cu/H-substituted solid solutions of **2**−**7** is attributed to the unique hydrogen bond character of the H atom.

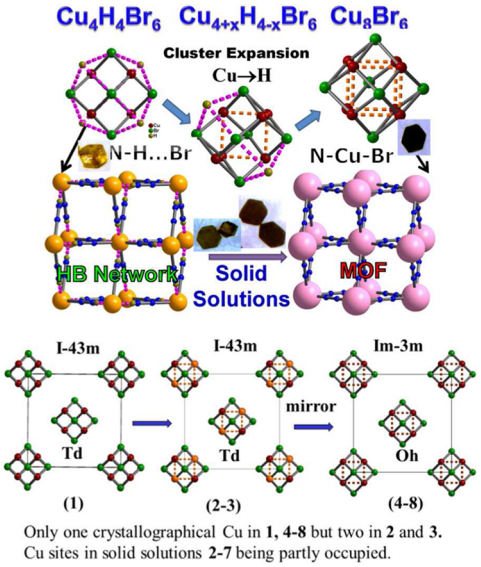

Figure 4. Schematic view of the crystal (top) and space group (bottom) transformation of the hydrogen bond network to a MOF via stepwise replacement of H atoms in N−H···Br bonds by Cu atoms accompanied by conversion of $[Cu_4(\mu_2\text{-}Br)_6]^{2-}$ to $[Cu_8(\mu_4\text{-}Br)_6]^{2+}$ cube clusters.

Synthesis Chemistry. Synthesis of **1**−**8** involves in situ reduction of Cu(II) to Cu(I) and decomposition of DMF to Me_2NH and formate. To understand the formation and crystallization mechanism, we compared and repeated many experiments. **1**−**8** are all available from the same starting materials with the same molar ratio at the same temperature of 85 °C; the reaction time is crucial to their formation and crystallization (Chart 2). When the reaction time was less than 48 h, only blue powders were obtained, corresponding to Cu(II) species. When the reaction time was increased to 48 h, a majority of tetranuclear Cu_4Br_6 cluster-based hydrogen bond network **1** and a minority of solid solution **2** were crystallized. Further increasing the reaction time resulted in the generation of solid solutions **3**−**7** and MOF **8**. Lastly, when the reaction time was increased to 360 h, single phase crystals of MOF **8** were generated. As demonstrated, a long time is necessary for the in situ reduction of Cu(II) to Cu(I) under synthetic conditions. Increasing the reaction temperature and utilizing a N-containing solvent can augment the reduction of Cu(II) to Cu(I) in a shorter amount of time. These observations indicated that tetranuclear cluster **1** and solid solutions **2**−**7** are less stable than 3D MOF **8**.

Chart 2. Relationship between Reaction Time and Products

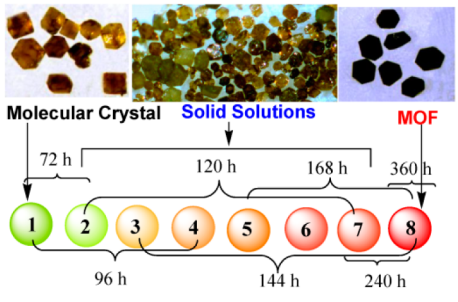

Mechanism of Crystal Growth and Evolution. Crystallization occurs at a kinetic equilibrium during which some less-stable crystals disappear and some more-stable crystals appear.[23] The observed phenomena herein are in agreement with the structural analyses of **1**−**8**. The N−H···Br and N−Cu−Br bonds have equivalent functionality with differing strengths. It seems that reduced Cu(I) atoms and bromides are first assembled into tetrahedral Cu_4Br_6 building units, which can be further coordinated by singly protonated HDABCO groups via Cu−N bonds. Each Cu_4Br_6 unit is coordinated by four HDABCO groups to form $[Cu_4Br_6(HDABCO)_4]^{2+}$ clusters that are linked together via self-complementary N−H···Br hydrogen bonds into the body-centered cubic hydrogen framework of **1**. Because the strength and stability of N−Cu−Br coordination bonds are larger than those of N−H···Br hydrogen bonds, the H atoms in N−H···Br bonds can be replaced by Cu(I) atoms in the presence of excess Cu(I) atoms in solution. With the stepwise replacement of H by Cu(I) atoms, solid solutions **2**−**7** are formed. Finally, when all H atoms in N−H···Br bonds have been replaced by Cu(I) atoms, MOF **8** is obtained and $[Cu_4Br_6]^{2-}$ tetrahedral clusters are transformed into $[Cu_8Br_6]^{2+}$ cube clusters. In principle, the formation of MOF **8** could be the result of direct assembly of Cu_8Br_6 cubes and bifunctional DABCO groups via Cu−N bonds. However, the absence of crystals of **8** formed within the initial 48 h does not support this hypothesis. The formation of solid solutions **2**−**7** and MOF **8** can be achieved by the postsynthesized treatment of **1** in a parent solution. This indicates that the evolution of **1** to **2**−**8** follows the mechanism of crystal to crystal transformation.

To understand the driving force behind N−Cu−Br bonds substituting for N−H···Br hydrogen bonds and the corresponding transformation from **1** to **2**−**8**, DFT calculations were performed with the Gaussian09 suite of programs. We selected fragment model $Cu_4Br_6HNMe_3$ as the reactant (Figure 5), in which H from $HNMe_3$ is triply hydrogen bonded to Br atoms. This model is in agreement with the local environment of the H atom in the N−H···Br bond in **1**. Fragment $Cu_5Br_6NMe_3$ is

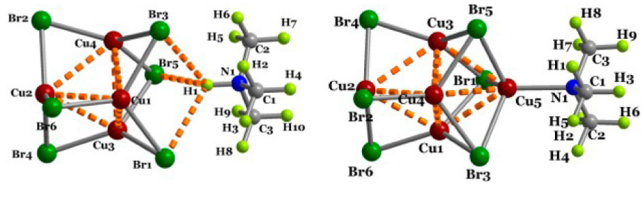

Figure 5. Optimized structures for reactant $Cu_4Br_6HNMe_3$ and product $Cu_5Br_6NMe_3$.

DOI: 10.1021/ic5024168
Inorg. Chem. 2015, 54, 554−559

representative of the product, in which the Cu atom that is coordinated to NMe_3 and three Br atoms could replicate the local coordination geometry of the Cu atom in **8**. Optimizations of these model fragments were computed using the B3LYP/6-311+G(d,p) method. Compared with the fragments in **1** and **8**, the optimized structures could reflect the local geometries of H and Cu atoms in **1** and **8**. However, as a result of the unsaturation of coordination of some Cu atoms, the neglect of seven additional N−H···Br hydrogen bonds, and the crystal field effect, the optimized structures are significantly shrunken, and the Cu···Cu distances are shorter by 1.07 Å. Interestingly, we found that the overall reaction $Cu_4Br_6HNMe_3$ + CuBr → $Cu_5Br_6NMe_3$ + HBr is exothermic by 22.31 kcal/mol (ΔH) and exergonic by 6.93 kcal/mol (ΔG). The calculated results suggest that the bonding energy gained can compensate for the bonding energy lost in the overall model reaction. As for the actual reaction, the transformation from $Cu_4Br_6HNMe_3$ to $Cu_5Br_6NMe_3$ will be more exothermic because of the greater number of fragments involved.

Photoluminescence. Remarkably, compounds **1**−**8** in the solid state at room temperature show strong and tunable photoluminescence. Upon excitation at 327 nm, molecular compound **1** shows a yellow emission with a maximum at 556 nm, and Cu_8Br_6 cube cluster-based MOF **8** shows red emission with a maximum at 644 nm. The mixture of solid solutions **2**−**7** shows tunable emissions in the range of 556−644 nm depending on their relative percentages (Figure 6). The

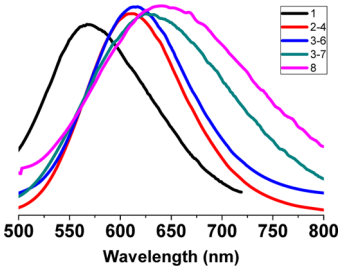

Figure 6. Photoluminescent emissions of **1**−**8** upon excitation at 327 nm.

lifetimes of the emission bands were measured to be on the level of microseconds, suggesting some character of phosphorescence. Compared to that of **1**, the maximum emission wavelength of **8** is red-shifted ∼88 nm.

Time-dependent DFT calculations have been used to analyze the luminescent origin of the complexes. The $[Cu_4Br_6]^{2-}$ and $[Cu_8Br_6]^{2+}$ models adapted from the X-ray data, as well as modified $[Cu_4Br_6(NH_3)_4]^{2-}$ (T_d) and $[Cu_8Br_6(NH_3)_4]^{2+}$ (O_h) models, have been optimized and used for calculations at the B3LYP level. Compared with experimental structures, the optimized tetranuclear $[Cu_4Br_6]^{2-}$ and $[Cu_4Br_6(NH_3)_4]^{2-}$ clusters show significant contraction, as demonstrated by short Cu···Cu distances of 2.89 Å. This means that $[Cu_4Br_6(HDABCO)_4]^{2+}$ clusters with large Cu···Cu distances of 3.97 Å in **1** are high-energy configurations that are stabilized by charge-assisted N−H···Br hydrogen bonds. For the $[Cu_8Br_6]^{2+}$ cube cluster, the optimized and experimental structures match well, as indicated by the calculated Cu···Cu distance of 2.87 Å (Figure 7). For the $[Cu_8Br_6(NH_3)_4]^{2+}$ cube cluster, the optimized structure with a Cu···Cu distance of 3.30 Å is largely in alignment with the experimental one. Agreement of experimental and calculated $[Cu_8Br_6]^{2+}$ and

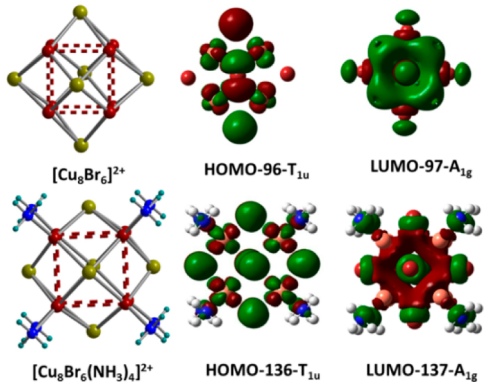

Figure 7. Optimized structural models for octanuclear $[Cu_8Br_6]^{2+}$ and $[Cu_8Br_6(NH_3)_4]^{2+}$ (O_h) and their frontier orbitals (isosurface value = 0.02 au).

$[Cu_8Br_6(NH_3)_4]^{2+}$ structures justifies the luminescence explanation. The calculated results indicate that all transitions in these complexes are qualitatively dominated by "cluster centered" excited states.[24] HOMOs in these models are composed of 3D orbitals of Cu(I) and 4p orbitals of the bromine atoms, whereas LUMOs mainly consist of 4s orbitals of copper with a minor admixture of 4p orbitals of the bromine atoms. The calculated transition in the $[Cu_8Br_6]^{2+}$ model complex has negligible oscillator strength (f), but significant oscillator strength of f = 0.0653 is found in the triply degenerated transition of the $[Cu_8Br_6(NH_3)_4]^{2+}$ model. The calculated excitation energy in $[Cu_8Br_6(NH_3)_4]^{2+}$ is 3.5428 eV (349.96 nm), which is close to the experimental value of 327 nm.

CONCLUSION

In summary, solvothermal reactions generated a series of body-centered cubic cuprous bromide networks. Surprisingly, despite very similar unit cell parameters, they evolve from discrete $[Cu_4(\mu\text{-Br})_6(HDABCO)_4]^{2+}$ cluster-based hydrogen networks to solid solutions $[Cu_{4+x}H_{4-x}Br_6(DABCO)_4]$ to an infinite $[Cu_8(\mu_4\text{-Br})_6]^{2+}$ cube cluster-based MOF. This work directly reveals not only the equivalence and transformation between N−H···Br hydrogen bonds and N−Cu−Br coordination bonds but also the seemingly impossible phenomenon of Cu/H-substituted solid solutions. Meanwhile, it also marries molecular and coordination crystal engineering, two different sub-areas of crystal engineering. Stoichiometry of CuBr in these networks can be tuned from Cu_4Br_6 to Cu_8Br_6 via $Cu_{4+x}Br_6$ ($0 < x < 4$), and strong, tunable emissions from yellow to red have been observed. Stabilization of the seemingly unstable high-energy $[Cu_4Br_6(HDABCO)_4]^{2+}$ configuration with a large Cu···Cu distance of 3.97 Å is attributed to N−H···Br hydrogen bonds. Superior properties of multicomponent solids are also demonstrated by tunable photoluminescence. This work reveals that equivalent replacement of N−H···Br hydrogen bonds by N−Cu−Br coordination bonds could be a superior method for multicomponent solids.

ASSOCIATED CONTENT

Supporting Information

Crystal data in CIF, crystal images, infrared spectra, XRPD, additional structural figures, optimized structural models for $Cu_4Br_6^{2-}$ clusters, as well as frontier orbitals, TGA curves, and EDS plots. This material is available free of charge via the Internet at http://pubs.acs.org.

DOI: 10.1021/ic5024168
Inorg. Chem. 2015, 54, 554−559

AUTHOR INFORMATION

Corresponding Author

*E-mail: zhangxm@dns.sxnu.edu.cn.

Notes

The authors declare no competing financial interest.

ACKNOWLEDGMENTS

This work was supported by the 973 Program (2012CB821701), the Ministry of Education of China (Grant IRT1156), and the National Science Fund for Distinguished Young Scholars (Grant 20925101).

REFERENCES

(1) O'Keeffe, M.; Yaghi, O. M. *Chem. Rev.* **2012**, *112*, 675−702.

(2) (a) Bétard, A.; Fischer, R. A. *Chem. Rev.* **2012**, *112*, 1055−1083. (b) Cui, Y.; Yue, Y.; Qian, G.; Chen, B. *Chem. Rev.* **2012**, *112*, 1126−1162. (c) Gagnon, K. J.; Perry, H. P.; Clearfield, A. *Chem. Rev.* **2012**, *112*, 1034−1054. (d) Getman, R. B.; Bae, Y.-S.; Wilmer, C. E.; Snurr, R. Q. *Chem. Rev.* **2012**, *112*, 703−723. (e) Horcajada, P.; Gref, R.; Baati, T.; Allan, P. K.; Maurin, G.; Couvreur, P.; Férey, G.; Morris, R. E.; Serre, C. *Chem. Rev.* **2012**, *112*, 1232−1268. (f) Kreno, L. E.; Leong, K.; Farha, O. K.; Allendorf, M.; Van Duyne, R. P.; Hupp, J. T. *Chem. Rev.* **2012**, *112*, 1105−1125. (g) Suh, M. P.; Park, H. J.; Prasad, T. K.; Lim, D.-W. *Chem. Rev.* **2012**, *112*, 782−835. (h) Sumida, K.; Rogow, D. L.; Mason, J. A.; McDonald, T. M.; Bloch, E. D.; Herm, Z. R.; Bae, T.-H.; Long, J. R. *Chem. Rev.* **2012**, *112*, 724−781. (i) Wang, C.; Zhang, T.; Lin, W. *Chem. Rev.* **2012**, *112*, 1084−1104. (j) Wu, H.; Gong, Q.; Olson, D. H.; Li, J. *Chem. Rev.* **2012**, *112*, 836−868. (k) Yoon, M.; Srirambalaji, R.; Kim, K. *Chem. Rev.* **2012**, *112*, 1196−1231. (l) Zhang, J.-P.; Zhang, Y.-B.; Lin, J.-B.; Chen, X.-M. *Chem. Rev.* **2012**, *112*, 1001−1033. (m) Zhang, W.; Xiong, R.-G. *Chem. Rev.* **2012**, *112*, 1163−1195. (n) Allendorf, M. D.; Bauer, C. A.; Bhakta, R. K.; Houk, R. J. T. *Chem. Soc. Rev.* **2009**, *38*, 1330−1352. (o) Czaja, A. U.; Trukhan, N.; Müller, U. *Chem. Soc. Rev.* **2009**, *38*, 1284−1293. (p) Düren, T.; Bae, Y.-S.; Snurr, R. Q. *Chem. Soc. Rev.* **2009**, *38*, 1237−1247. (q) Férey, G.; Serre, C. *Chem. Soc. Rev.* **2009**, *38*, 1380−1399. (r) Paz, F. A.; Klinowski, J.; Vilela, S. M.; Tome, J. P.; Cavaleiro, J. A.; Rocha, J. *Chem. Soc. Rev.* **2012**, *41*, 1088−1110. (s) Perry, J. J., IV; Perman, J. A.; Zaworotko, M. J. *Chem. Soc. Rev.* **2009**, *38*, 1400−1417. (t) Spokoyny, A. M.; Kim, D.; Sumrein, A.; Mirkin, C. A. *Chem. Soc. Rev.* **2009**, *38*, 1218−1227. (u) Uemura, T.; Yanai, N.; Kitagawa, S. *Chem. Soc. Rev.* **2009**, *38*, 1228−1236. (v) Wang, Z.; Cohen, S. M. *Chem. Soc. Rev.* **2009**, *38*, 1315−1329. (w) Zacher, D.; Shekhah, O.; Woll, C.; Fischer, R. A. *Chem. Soc. Rev.* **2009**, *38*, 1418−1429. (x) Parnham, E. R.; Morris, R. E. *Acc. Chem. Res.* **2007**, *40*, 1005−1013. (y) Kitagawa, S.; Kitaura, R.; Noro, S.-I. *Angew. Chem., Int. Ed.* **2004**, *43*, 2334−2375. (z) Furukawa, H.; Cordova, K. E.; O'Keeffe, M.; Yaghi, O. M. *Science* **2013**, *341*, 1230444. (aa) Xi, X.; Fang, Y.; Dong, T.; Cui, Y. *Angew. Chem., Int. Ed.* **2011**, *50*, 1154−1158.

(3) (a) Cohen, S. M. *Chem. Rev.* **2012**, *112*, 970−1000. (b) Stock, N.; Biswas, S. *Chem. Rev.* **2012**, *112*, 933−969. (c) Kole, G. K.; Vittal, J. J. *Chem. Soc. Rev.* **2013**, *42*, 1755−1775. (d) MacGillivray, L. R.; Papaefstathiou, G. S.; Friščić, T.; Hamilton, T. D.; Bučar, D.-K.; Chu, Q.; Varshney, D. B.; Georgiev, I. G. *Acc. Chem. Res.* **2008**, *41*, 280−291. (e) Li, L.; Xiang, S.; Cao, S.; Zhang, J.; Ouyang, G.; Chen, L.; Su, C.-Y. *Nat. Commun.* **2013**, *4*, 1774. (f) Jing, X.; He, C.; Dong, D.; Yang, L.; Duan, C. *Angew. Chem., Int. Ed.* **2012**, *51*, 10127−10131.

(4) (a) Wang, C.; Liu, D.; Lin, W. *J. Am. Chem. Soc.* **2013**, *135*, 13222−13234. (b) Wang, Z.; Cohen, S. M. *J. Am. Chem. Soc.* **2007**, *129*, 12368−12369. (c) Wang, B.; Cote, A. P.; Furukawa, H.; O'Keeffe, M.; Yaghi, O. M. *Nature* **2008**, *453*, 207−212. (d) Banerjee, R.; Phan, A.; Wang, B.; Knobler, C.; Furukawa, H.; O'Keeffe, M.; Yaghi, O. M. *Science* **2008**, *319*, 939−944. (e) Eddaoudi, M.; Kim, J.; Rosi, N.; Vodak, D.; Wachter, J.; O'Keeffe, M.; Yaghi, O. M. *Science* **2002**, *295*, 469−472. (f) He, L.; Liu, Y.; Liu, J.; Xiong, Y.; Zheng, J.; Liu, Y.; Tang, Z. *Angew. Chem., Int. Ed.* **2013**, *52*, 3741−3745. (g) Yang, S.; Sun, J.; Ramirez-Cuesta, A. J.; Callear, S. K.; David, W. I.; Anderson, D. P.; Newby, R.; Blake, A. J.; Parker, J. E.; Tang, C. C.; Schroder, M. *Nat. Chem.* **2012**, *4*, 887−894. (h) Zhang, J.; Wu, T.; Zhou, C.; Chen, S.; Feng, P.; Bu, X. *Angew. Chem., Int. Ed.* **2009**, *48*, 2542−2545.

(5) Murugavel, R.; Walawalkar, M. G.; Dan, M.; Roesky, H. W.; Rao, C. N. R. *Acc. Chem. Res.* **2004**, *37*, 763−774.

(6) (a) Desiraju, G. R. *Angew. Chem., Int. Ed.* **2007**, *46*, 8342−8356. (b) Brammer, L. *Chem. Soc. Rev.* **2004**, *33*, 476−489. (c) Li, J.-R.; Timmons, D. J.; Zhou, H.-C. *J. Am. Chem. Soc.* **2009**, *131*, 6368−6369.

(7) Tiekink, E. R., Vittal, J. J., Eds. *Frontiers in Crystal Engineering*; Wiley & Sons: West Sussex, U.K., 2006.

(8) (a) Karagiaridi, O.; Bury, W.; Tylianakis, E.; Sarjeant, A. A.; Hupp, J. T.; Farha, O. K. *Chem. Mater.* **2013**, *25*, 3499−3503. (b) Gui, B.; Hu, G.; Zhou, T.; Wang, C. *J. Solid State Chem.* **2014**, DOI: 10.1016/j.jssc.2014.06.023.

(9) (a) Das, S.; Kim, H.; Kim, K. *J. Am. Chem. Soc.* **2009**, *131*, 3814−3815. (b) Burnett, B. J.; Barron, P. M.; Hu, C.; Choe, W. *J. Am. Chem. Soc.* **2011**, *133*, 9984−9987. (c) Brozek, C. K.; Dincă, M. *J. Am. Chem. Soc.* **2013**, *135*, 12886−12891.

(10) (a) Adisoejoso, J.; Tahara, K.; Okuhata, S.; Lei, S.; Tobe, Y.; De Feyter, S. *Angew. Chem., Int. Ed.* **2009**, *48*, 7353−7357. (b) Bolton, O.; Matzger, A. J. *Angew. Chem., Int. Ed.* **2011**, *50*, 8960−8963. (c) Khan, M.; Enkelmann, V.; Brunklaus, G. *J. Am. Chem. Soc.* **2010**, *132*, 5254−5263.

(11) (a) Burrows, A. D. *CrystEngComm* **2011**, *13*, 3623−3642. (b) Atkinson, M. B.; Mariappan, S. V.; Bucar, D. K.; Baltrusaitis, J.; Friscic, T.; Sinada, N. G.; MacGillivray, L. R. *Proc. Natl. Acad. Sci. U.S.A.* **2011**, *108*, 10974−10979.

(12) Kusada, K.; Yamauchi, M.; Kobayashi, H.; Kitagawa, H.; Kubota, Y. *J. Am. Chem. Soc.* **2010**, *132*, 15896−15898.

(13) Fukushima, T.; Horike, S.; Inubushi, Y.; Nakagawa, K.; Kubota, Y.; Takata, M.; Kitagawa, S. *Angew. Chem., Int. Ed.* **2010**, *49*, 4820−4824.

(14) Deng, H.; Olson, M. A.; Stoddart, J. F.; Yaghi, O. M. *Nat. Chem.* **2010**, *2*, 439−443.

(15) Cotton, F. A.; Wilkinson, G.; Murillo, C. A.; Bochmann, M. *Advanced Inorganic Chemistry*; Wiley: New York, 1988; Vol. 5.

(16) Steiner, T. *Angew. Chem., Int. Ed.* **2002**, *41*, 48−76.

(17) Frisch, M. J.; Trucks, G. W.; Schlegel, H. B.; Scuseria, G. E.; Robb, M. A.; Cheeseman, J. R.; Scalmani, G.; Barone, V.; Mennucci, B.; Petersson, G. A.; Nakatsuji, H.; Caricato, M.; Li, X.; Hratchian, H. P.; Izmaylov, A. F.; Bloino, J.; Zheng, G.; Sonnenberg, J. L.; Hada, M.; Ehara, M.; Toyota, K.; Fukuda, R.; Hasegawa, J.; Ishida, M.; Nakajima, T.; Honda, Y.; Kitao, O.; Nakai, H.; Vreven, T.; Montgomery, J. A., Jr.; Peralta, J. E.; Ogliaro, F.; Bearpark, M.; Heyd, J. J.; Brothers, E.; Kudin, K. N.; Staroverov, V. N.; Kobayashi, R.; Normand, J.; Raghavachari, K.; Rendell, A.; Burant, J. C.; Iyengar, S. S.; Tomasi, J.; Cossi, M.; Rega, N.; Millam, M. J.; Klene, M.; Knox, J. E.; Cross, J. B.; Bakken, V.; Adamo, C.; Jaramillo, J.; Gomperts, R.; Stratmann, R. E.; Yazyev, O.; Austin, A. J.; Cammi, R.; Pomelli, C.; Ochterski, J. W.; Martin, R. L.; Morokuma, K.; Zakrzewski, V. G.; Voth, G. A.; Salvador, P.; Dannenberg, J. J.; Dapprich, S.; Daniels, A. D.; Farkas, Ö.; Foresman, J. B.; Ortiz, J. V.; Cioslowski, J.; Fox, D. J. *Gaussian09*; Gaussian, Inc.: Wallingford, CT, 2009.

(18) Andersson, S.; Jagner, S. *Acta Chem. Scand.* **1986**, *A40*, 210.

(19) Brammer, L.; Bruton, E. A.; Sherwood, P. *Cryst. Growth Des.* **2001**, *1*, 277−290.

(20) Luo, T. T.; Tsai, H. L.; Yang, S. L.; Liu, Y. H.; Yadav, R. D.; Su, C. C.; Ueng, C. H.; Lin, L. G.; Lu, K. L. *Angew. Chem., Int. Ed.* **2005**, *44*, 6063−6067.

(21) (a) Desiraju, G. R. *Acc. Chem. Res.* **2002**, *35*, 565−573. (b) Dalrymple, S. A.; Shimizu, G. K. *J. Am. Chem. Soc.* **2007**, *129*, 12114−12116.

(22) Peng, R.; Li, M.; Li, D. *Coord. Chem. Rev.* **2010**, *254*, 1−18.

(23) Jiang, J.-J.; He, J.-R.; Lu, X.-Q.; Wang, D.-W.; Li, G.-B.; Su, C.-Y. *IUCrJ* **2014**, *1*, 318−327.

(24) (a) Ford, P. C.; Cariati, E.; Bourassa, J. *Chem. Rev.* **1999**, *99*, 3625−3648. (b) Wing-Wah Yam, V.; Kam-Wing Lo, K. *Chem. Soc. Rev.* **1999**, *28*, 323−334.

DOI: 10.1021/ic5024168
Inorg. Chem. 2015, 54, 554−559